The real part of (A2) gives

$$\tau_A^r \delta A + \tau_\omega^r \frac{d\phi}{dt} + \frac{\tau_\omega^i}{A_0}\frac{d\delta A}{dt} = 0. \quad \text{(A4)}$$

By using (A3) form of $d\phi/dt$ into (A4):

$$\tau_A^r \delta A + \frac{\tau_\omega^r}{\tau_\omega^i}\left[\frac{\tau_\omega^r}{A_0}\frac{d\delta A}{dt} - \tau_A^i \delta A\right] + \frac{\tau_\omega^i}{A_0}\frac{d\delta A}{dt} = 0 \quad \text{(A5)}$$

$$\left(\tau_A^i - \frac{\tau_\omega^r}{\tau_\omega^i}\tau_A^i\right)\delta A + \left(\frac{\tau_\omega^i}{A_0} + \frac{(\tau_\omega^r)^2}{\tau_\omega^i A_0}\right)\frac{d\delta A}{dt} = 0 \quad \text{(A6)}$$

$$\frac{1}{\tau_\omega^i}[\tau_A^r\tau_\omega^i - \tau_\omega^r\tau_A^i]\,\delta A + \frac{1}{\tau_\omega^i A_0}[(\tau_\omega^i)^2 + (\tau_\omega^r)^2]\frac{d\delta A}{dt} = 0 \quad \text{(A7)}$$

if τ_ω^i is nonzero, multiply both sides by τ_ω^i, and use the imaginary operator:

$$\mathrm{Im}\left\{\left(\frac{\partial\tau}{\partial\omega}\right)\left(\frac{\partial\tau}{\partial A}\right)^*\right\}\delta A + \frac{1}{A_0}\left|\frac{\partial\tau}{\partial\omega}\right|^2\frac{d\delta A}{dt} = 0 \quad \text{(A8)}$$

$$A_0\left|\frac{\partial\tau}{\partial\omega}\right|^{-2}\mathrm{Im}\left\{\left(\frac{\partial\tau}{\partial\omega}\right)\left(\frac{\partial\tau}{\partial A}\right)^*\right\}\delta A + \frac{d\delta A}{dt} = 0 \quad \text{(A9)}$$

Acknowledgment

The authors thank P. M. Smith of GE for his advice and encouragement.

References

[1] M. J. Howes and D. V. Morgan, *Microwave Devices*. New York: Wiley, 1976, pp. 209–217.
[2] J. Millman, *Microelectronics*. New York: McGraw-Hill, 1979, pp. 647–648.
[3] D. J. Esdale and M. J. Howes, "A reflection coefficient approach to the design of one-port negative impedance oscillators," *IEEE Trans. Microwave Theory Tech.*, vol. MTT-29, no. 8, pp. 770–776, Aug. 1981.
[4] G. R. Basawapatna and R. B. Stancliff, "A unified approach to the design of wide-band microwave solid-state oscillators," *IEEE Trans. Microwave Theory Tech.*, vol. MTT-27, no. 5, pp. 379–385, May 1979.
[5] G. D. Vendelin, *Design of Amplifiers and Oscillators by the S-Parameter Method*. New York: Wiley, 1982, pp. 132–172.
[6] K. Kurokawa, "Injection locking of microwave solid-state oscillators," *Proc. IEEE*, vol. 61, no. 10, pp. 1386–1410, Oct. 1973.
[7] A. I. Mees and L. O. Chua, "The Hopf bifurcation theorem and its applications to nonlinear oscillations in circuits and systems," *IEEE Trans. Circuits Syst.*, vol. CAS-26, no. 4, pp. 235–254, Apr. 1979.
[8] D. J. Allwright, "Harmonic balance and the Hopf bifurcation," *Mathematical Proceedings of the Cambridge Philosophical Society*, vol. 82, pp. 453–467, 1977.
[9] S. J. Mason, "Feedback theory-further properties of signal flow graphs," *Proc. IRE*, vol. 44, pp. 920–926, July 1956.
[10] G. Gonzalez, *Microwave Transistor Amplifiers*. Englewood Cliffs, NJ: Prentice-Hall, 1984, pp. 194–199.
[11] S. M. Sze, *Physics of Semiconductor Devices*, 2nd ed. New York: Wiley, 1981, pp. 637–642.
[12] R. A. Pucel, R. Bera, and D. Masse, "Experiments on integrated gallium-arsenide FET oscillators at X-band," *Electron. Lett.*, vol. 11, no. 10, pp. 219–220, May 15, 1975.
[13] K. M. Johnson, "Large signal GaAs MESFET oscillator design," *IEEE Trans. Microwave Theory Tech.*, vol. MTT-27, no. 3, pp. 217–226, Mar. 1979.

Parameter Extraction Technique for HBT Equivalent Circuit Using Cutoff Mode Measurement

Seonghearn Lee and Anand Gopinath

Abstract—**We propose a new parameter extraction method based on the *S*-parameter measurements of the HBTs biased to cutoff. This method is applied to confirm the results for the RF probe pad and interconnection pattern parasitics obtained from the special test structures, and to determine some of the device capacitances of the HBT. The remaining device parameters are extracted by the *S*-parameter measurements of the devices biased to the active mode. The extraction technique gives good agreement between the equivalent circuit and the measured *S*-parameters of the HBT including probe pads and interconnections.**

I. Introduction

Heterojunction bipolar transistors (HBT's) are used in monolithic microwave integrated circuit (MMIC) applications. Accurate parameter extraction of their equivalent circuit is crucial for the development of HBT circuits and applications. These device equivalent circuits are derived from scattering (*S*)-parameter measurements [1]–[7] usually measured on discrete devices using "on wafer" RF probes over a range of frequencies and biases. For the "on wafer" probing, the additional RF probe pads and interconnections (RF probe-pattern) have to be added to the device, and their parasitics are included in the measurement. Computer optimization is used to fit the equivalent circuit parameters together with parasitics, to the measured *S*-parameters [5]–[7]. In general, it is necessary to reduce the number of unknown parameters to avoid the non-physical local minima which occur in this technique [7]. Thus, experimental determination of the parasitic parameters is the best method to achieve this reduction of the parameter space dimension. Usually, the RF probe-pattern (pads and interconnections) parasitics are ignored, and as a result, the agreement between the circuit *S*-parameters and measurements is often not very good. It is therefore necessary that an equivalent circuit model including the RF probe-pattern be used in this parameter extraction process.

In general, most of the equivalent circuit modeling results have been optimized without independent measurements of probe-pattern parasitics. RF probe-pattern parasitics may be predetermined by means of properly designed test structures [1], [8]. In a previous paper [9], we have introduced an accurate parameter extraction scheme for RF probe-pattern parasitics using the simultaneous optimization of "open" and "short" test structures. We have also proposed a new RF probe-pattern equivalent circuit model, and have demonstrated that this model overcomes some of the shortcoming of previous models [1], [2].

Fig. 1 shows the layout of a typical RF probe-pattern used to measure HBT's built at the University of Minnesota. The RF probe-pattern parasitics are determined by measuring two test structures, as discussed previously [9]: one is an "open" circuit structure that consists of RF probe pads and interconnections on the appropriate passivation layer (silicon nitride in our case), and the other is a

Manuscript received May 13, 1991; revised September 3, 1991.
The authors are with the Department of Electrical Engineering, University of Minnesota, 200 Union Street, S.E., Minneapolis, MN 55455.
IEEE Log Number 9105453.

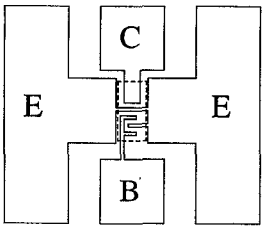

Fig. 1. The layout of a typical RF probe-pattern used for "on wafer" measurements for our HBT's. The dashed box represents the HBT.

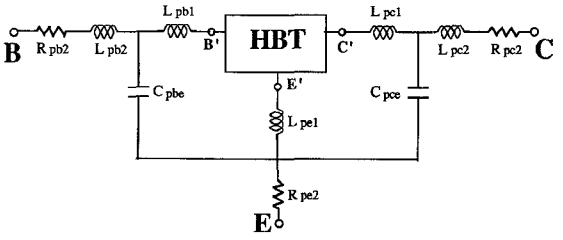

Fig. 2. An equivalent circuit model representing RF probe-pattern.

"short" circuit test structure that includes RF probe pads, interconnections, and gold lines to short the three open circuit interconnection terminals at the plane of HBT. A probe-pattern equivalent circuit model for the RF probe pads and interconnections, shown in Fig. 2, has been proposed previously [9], as previous models [1], [2] are not adequate. In general, the probe-pattern is a combination of several transmission lines with additional strays which include distributed capacitances, inductances, and resistances. In the limit, transmission lines of various lengths and impedances, with additional stray capacitances would be the closest representation to reality, but it is often preferable to model these with lumped elements, as shown in Fig. 2.

In this paper, a cutoff-mode technique with the HBT biased to cutoff is developed to confirm the results of the previous method of RF probe-pattern parasitics, and also to determine some of the capacitances of the device. Subsequently, further optimization is then performed using measurements with the device biased to the activity, to extract the remaining device parameters.

II. Parameter Extraction Using Cutoff Mode Measurement

To confirm the probe-pattern equivalent circuit values obtained previously [9] from "open" and "short" test structures, we repeat the *S*-parameter measurements on the device with the same RF probe-pattern, biased to cutoff. This cutoff mode technique is similar to the "cold FET modeling" [10], [11] used for MESFET's. In this cutoff mode, the intrinsic device is modeled by simple passive circuit consisting of the emitter-base (E-B) and the base-collector (B-C) depletion capacitances, because E-B and B-C junctions are reverse-biased together with the probe-pattern parasitics.

The cutoff mode *S*-parameters from 0.045 to 26.5 GHz are measured on several n-p-n AlGaAs/GaAs thick base HBT's (used for minority carrier mobility measurements [12]) with emitter area of $8.0 \times 8.0\ \mu m^2$, biased at $V_{CB} = 3.1$ V and $V_{BE} = -1.0$ V using the same RF probe-pattern discussed above. Table I shows the epitaxial layer structure for fabricated HBT's. This structure was grown by MBE on a semi-insulating GaAs substrate. Ni/Ge/Au was evaporated as emitter and collector ohmic contacts. For the

TABLE I
Epitaxial Layer Structure for Fabricated Thick-Base HBT

Layer	Material	AlAs Fraction	Doping (cm^{-3})	Thickness (Å)
Contact (1)	n^+-GaAs		6×10^{18}	1500
Contact (2)	n-GaAs		6×10^{17}	500
Emitter (1)	n-AlGaAs	0–0.3	2×10^{17}	500
Emitter (2)	n-AlGaAs	0.3	2×10^{17}	3000
Spacer	GaAs			100
Base	p^+-GaAs		3×10^{19}	7000
Collector	n-GaAs		5×10^{15}	11 500
Buffer	n^+-GaAs		6×10^{18}	10 000
Substrate	S. I. GaAs			

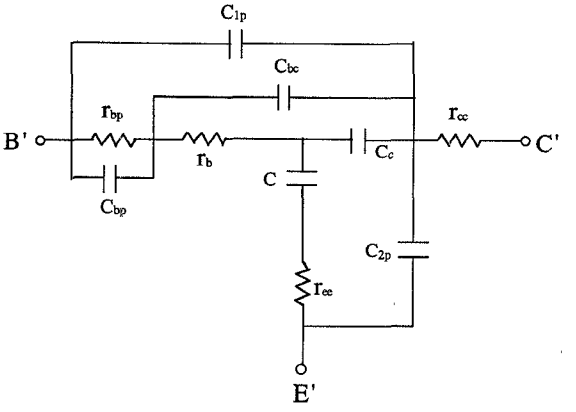

Fig. 3. Cutoff-mode small signal equivalent circuit of HBT at $V_{CB} = 3.1$ V and $V_{BE} = -1.0$ V.

base contact, Ti/Pt/Au was used in our HBT process. This device was fabricated by using $NH_4OH/H_2O_2/H_2O$ solution for all mesa and isolation etching. The base surface is covered by a thin depleted AlGaAs cap layer to reduce the surface recombination effects [13]. PE-CVD silicon nitride films were deposited for the device passivation.

The HBT cutoff mode equivalent circuit of a typical device without RF probe-pattern is shown in Fig. 3. This equivalent circuit consists of the intrinsic device capacitance (C_c), the extrinsic device parasitics (r_b, r_{bp}, r_{cc}, r_{ee}, C_{bc}, and C_{bp}), and capacitances (C_{1p}, C_{2p}) due to passivation layer (silicon nitride) between interconnection metals and n^+ collector contact layer. In this model, C_c is the intrinsic base-collector junction capacitance, C_{bc} is the extrinsic base-collector junction capacitance, r_b is the intrinsic base resistance, r_{cc} is the collector resistance, r_{ee} is the emitter resistance including the contact resistance, r_{bp} is the base contact resistance, and C_{bp} is the base contact capacitance [1]. The cutoff mode model was optimized to minimize the error between modeled and measured *S*-parameters using the EEsof Touchstone computer-aided microwave simulation and optimization program [14] until no further change in the parameter values is seen, and shows good agreement with measured *S*-parameters. Since the equivalent circuit of the cutoff mode HBT is simpler than that of the active mode, a cutoff mode optimization allows us to extract some of HBT parameters with great accuracy. The probe-pattern parasitics obtained from test structures have uncertainties due to errors associated with the inductances and resistances of gold lines in the "short" test pattern, and extra fringe capacitances in the "open" test pattern. In order to eliminate these uncertainties, during cutoff mode optimization,

values of all probe-pattern parasitics extracted from test structures are used as initial values, and permitted to vary within specified bounds. All probe-pattern parasitics and some device capacitances (C_c, C_{bc}, C_{1p}, and C_{2p}) may be determined accurately in the cutoff optimization. However, some of the HBT parameters (C_{bp}, r_b, r_{bp}, r_{cc}, and r_{ee}) are not accurate because their values are different in the active mode, due to their dependence on the device current [15].

III. Parameter Extraction Using Active Mode Measurement

For the HBT equivalent circuit in active mode, the intrinsic device elements (C_e, r_e, and A) are added to cutoff mode circuit, as shown in Fig. 4. In this circuit model, C_e is the emitter-base junction and diffusion capacitance, r_e is the dynamic emitter resistance, and A is the common-base current gain. The current gain is expressed as

$$A = A_o \left[\frac{e^{-j2\pi f \tau_d}}{1 + jf/f_\alpha} \right]$$

where A_o is the dc current gain, τ_d is the transit time, and f_α is the 3 dB frequency for current gain.

The S-parameter measurements for HBT's in the active mode together with same RF pad-pattern were performed on the same HBT's at $I_c = 2.6$ mA and $V_{CE} = 5.0$ V ($V_{CB} = 3.1$ V) using same experimental setup. In order to compensate the possible errors associated with cutoff mode biasing and measurement, this active mode equivalent circuit was next optimized to obtain the closest possible fit to the measured S-parameters while all pad-pattern parasitics and device capacitances (C_c, C_{bc}, C_{1p}, and C_{2p}) obtained from the cutoff optimization are used as initial values and varied with small bounds. These final optimized values show only small deviations from the initial values. Table II shows the extracted parameter values of the full equivalent circuit, which contains our HBT and the RF probe-pattern. The calculated S-parameters of the active mode equivalent circuit including RF probe-pattern parasitics using the entire set of parameter values in Table II, are compared with the measured S-parameters in Fig. 5, and show excellent agreement.

In order to investigate the physical validity of the extracted device parameter values, device parameters were calculated with theoretical methods [16], [17]. The approximate calculations give: $C_c \approx 6.7$ fF, $C_{bc} \approx 40$ fF, $C_{1p} \approx 29$ fF, $C_{2p} \approx 30$ fF, $r_b \approx 15\ \Omega$, and $r_e \approx 5.7\ \Omega$. The value of $r_{ee} \approx 40\ \Omega$ is obtained from the open-collector method [18]. A_o is found to be 0.565 from dc measurement. Good agreement between the extracted device parameters and these calculated (or dc-measured) values is obtained from this parameter extraction technique. However, $C_{2p} = 119$ fF which is larger than the calculated value may be due to the fringing capacitance associated with proximity of grounded emitter pad and n^+ collector contact layer. The extracted value of r_b which is smaller than 15 Ω may be due to the current crowding [19]. From these comparisons between extracted and calculated (or dc-measured) values, it is found that these parameter values extracted from our technique are physically acceptable.

IV. Conclusion

The uncertainties of the values of RF probe-pattern (RF probe pads and interconnections) parasitics extracted from "open" and "short" test structures in a previous paper [9] are first removed from a new parameter extraction technique based on S-parameter measurement of HBT's biased to the cutoff mode. The other un-

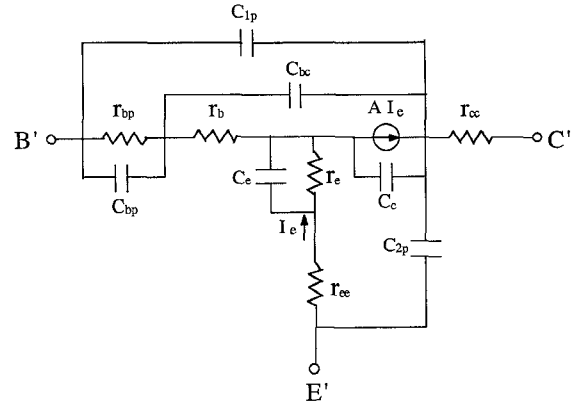

Fig. 4. Active-mode small signal equivalent circuit of HBT at $Ic = 2.6$ mA and $V_{CE} = 5.0$ V ($V_{CB} = 3.1$ V).

TABLE II
Extracted Small Signal Model Parameters of Our HBT and RF Probe Pattern

L_{pb1}	153 pH	r_{bp}	50.6 Ω
L_{pc1}	176 pH	r_{ee}	41.3 Ω
L_{pe1}	50.0 pH	r_{cc}	5.33 Ω
L_{pb2}	89.5 pH	C_e	4.19 pF
L_{pc2}	61.4 pH	C_c	12.5 fF
R_{pb2}	3.80 Ω	C_{bc}	33.8 fF
R_{pc2}	1.46 Ω	C_{bp}	296 fF
R_{pe2}	7.07 Ω	C_{1p}	23.7 fF
C_{pbe}	122 fF	C_{2p}	119 fF
C_{pce}	95.4 fF	A_o	0.576
r_e	5.73 Ω	τ_d	5.00 ps
r_b	10.0 Ω	f_α	6.27 GHz

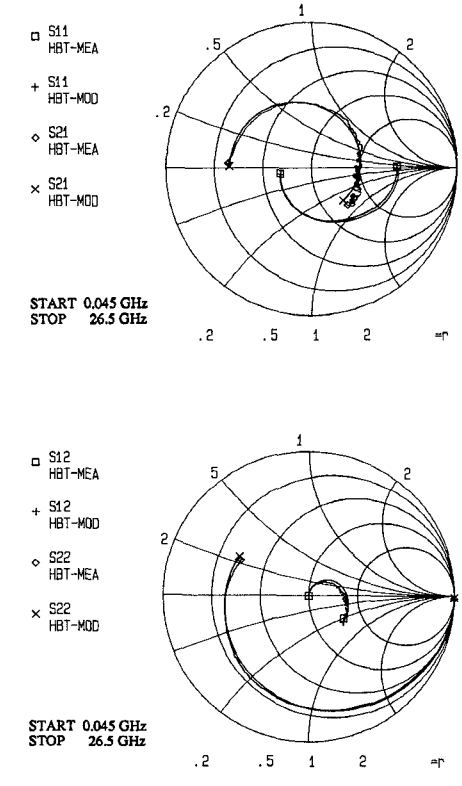

Fig. 5. Comparison between measured (HBT-MEA) and modeled (HBT-MOD) S-parameters of the HBT including RF probe-pattern in the frequency of 0.045 to 26.5 GHz.

certainties of probe-pattern parasitics and device capacitances determined from the previous cutoff technique, due to cutoff biasing, are eliminated by the optimization of HBTs in the active mode. The remainder of the device parameters are determined from the active mode optimization. The HBT equivalent circuit including a RF probe pad and interconnection circuit model determined from these techniques shows good agreement with measured S-parameters, while providing physically acceptable circuit parameter values. The extrinsic device de-embedded from probe-pattern parasitics may be used in circuit design programs.

ACKNOWLEDGMENT

The authors would like to thank B. J. Moon and Z. Abid for helpful discussions.

REFERENCES

[1] D. Costa, W. Liu, and J. S. Harris, Jr., "A new direct method for determining the heterojunction bipolar transistor equivalent circuit model," in *Proc. 1990 IEEE Bipolar Circuits and Technology Meeting*, pp. 118–121.

[2] M. E. Kim, A. K. Oki, J. B. Camou, P. D. Chow, B. L. Nelson, D. M. Smith, J. C. Canyon, C. C. Yang, R. Dixit, and B. R. Allen, "12–40 GHz low harmonic distortion and phase noise performance of GaAs heterojunction bipolar transistors," in *1988 IEEE GaAs IC Symp. Dig.*, pp. 117–120.

[3] B. Bayraktaroglu, and R. D. Hudgens, M. A. Khatibzadeh, and H. Q. Tserng, "2.5 W CW X-Band heterojunction bipolar transistor," in *1989 IEEE MTT-S Int. Microwave Symp. Dig.*, pp. 1057–1060.

[4] B. Bayraktaroglu, N. Camilleri, and S. A. Lambert, "Microwave performances of n-p-n and p-n-p AlGaAs/GaAs heterojunction bipolar transistors," *IEEE Trans. Microwave Theory Tech.*, vol. 36, pp. 1869–1873, 1988.

[5] U. K. Mishra, J. F. Jensen, D. B. Rensch, A. S. Brown, W. E. Stanchina, R. J. Trew, M. W. Pierce, and T. V. Kargodorian, "Self-aligned AlInAs-GaInAs heterojunction bipolar transistors and circuits," *IEEE Electron Device Lett.*, vol. 10, pp. 467–469, 1989.

[6] R. J. Trew, U. K. Mishra, and W. L. Pribble, "A parameter extraction technique for heterojunction bipolar transistors," in *1989 IEEE MTT-S Int. Microwave Symp. Dig.*, pp. 897–900.

[7] G. L. Bilbro, M. B. Steer, R. J. Trew, C. R. Chang, and S. G. Skaggs, "Extraction of the parameters of equivalent circuits of microwave transistors using tee annealing," *IEEE Trans. Microwave Theory Tech.*, vol. 38, pp. 1381–1390, 1990.

[8] P. J. van Wijnen, H. R. Claessen, and E. A. Wolsheimer, "A new straightforward calibration and correction procedure for "On wafer" high frequency S-parameter measurements (45 MHz–18 GHz)," in *Proc. 1987 IEEE Bipolar Circuits and Technology Meeting*, pp. 70–73.

[9] S. Lee and A. Gopinath, "New circuit model for RF probe pads and interconnections for the extraction of HBT equivalent circuit," *IEEE Electron Device Lett.*, vol. 12, pp. 521–523, 1991.

[10] F. Diamant and M. Laviron, "Measurement of the extrinsic series elements of a microwave MESFET under zero current condition," in *Proc. 12th European Microwave Conf.*, 1982, pp. 451–456.

[11] W. R. Curtice and R. L. Camisa, "Self-consistent GaAs FET models for amplifier design and device diagnostics," *IEEE Trans. Microwave Theory Tech.*, vol. MTT-32, pp. 1573–1578, 1984.

[12] M. I. Nathan, W. P. Dumke, K. Wrenner, S. Tiwari, S. L. Wright, and K. A. Jenkins, "Electron mobility in p-type GaAs," *Appl. Phys. Lett.*, vol. 52, pp. 654–656, 1988.

[13] H. H. Lin and S. C. Lee, "Super-gain AlGaAs/GaAs heterojunction bipolar transistor using an emitter edge-thinning design," *Appl. Phys. Lett.*, vol. 47, pp. 839–841, 1985.

[14] *EEsof Touchstone Reference Manual*, version 1.7, EEsof Inc., 1989.

[15] W. M. C. Sansen and R. G. Meyer, "Characterization and measurement of the base and emitter resistances of bipolar transistor," *IEEE J. Solid-State Circuits*, vol. SC-7, pp. 492–498, 1972.

[16] S. M. Sze, *Physics of Semiconductor Devices*, 2nd ed. New York: Wiley, 1981, pp. 33.

[17] M. B. Das, "High-frequency performance limitations of millimeter-wave heterojunction bipolar transistors," *IEEE Trans. Electron Devices*, vol. 35, pp. 604–614, 1988.

[18] I. E. Getreu, *Modeling the Bipolar Transistor*. Amsterdam: Elsevier, 1978, pp. 140–143.

[19] A. Neugroschel, "Measurement of the low-current band and emitter resistances of bipolar transistors," *IEEE Trans. Electron Devices*, vol. 34, pp. 817–822, 1987.

An Analysis of a Coupled-Ring Rotary Joint Design

E. D. Evans

***Abstract*—This paper describes a theoretical and experimental analysis of a coupled-ring rotary joint design. A rotary joint of this type is commonly used for mechanically scanned, multichannel radars. The main goal of the analysis is to develop a better understanding for the transfer of energy through the joint's highly coupled rings. We first consider the geometry of a typical single channel and then describe a coupled transmission line model for the coupled-ring network. Using the model, we determine the type of ring network needed for low channel loss and small rotational variations of this loss. A series of measurements on some test models support the predictions of the analysis.**

I. INTRODUCTION

Many radar systems use multichannel rotary joints to allow mechanical scanning of the radar beam in azimuth or elevation. More recent radar designs require rotary joints with higher powers and larger numbers of channels to achieve new range and beamforming requirements. Because of these new requirements, multichannel rotary joints must be carefully designed to achieve low channel loss and small rotational variations of this loss.

In this paper a theoretical model for the performance of a coupled-ring rotary joint is derived. This type of rotary joint is commonly used in radars that have more than five or six channels. The theoretical approach uses coupled transmission line theory to model the transfer of energy across the joint's highly coupled rings. Using the model, we calculate the effect of the coupled-ring network on the joint's power transmission coefficient. To check the predictions of the theory, we also measure the performance of some rotary joint test models.

Fig. 1 shows a cross section view and an expanded three-dimensional view of a typical coupled-ring rotary joint channel. The single channel consists of a stationary stator section and a rotating rotor section. The channel has a pancake shape that can be stacked for multichannel systems, and the ring design allows a hole through the center of the joint for passing cables to the multiple channels. The key components of the single channel are the stator and rotor coupling rings. The rings sit in a ring cavity and are positioned very closely together to allow strong capacitive coupling. The circumference of the rings is usually under a wavelength, and the size of the ring cavity is small enough to prevent the propagation of any coaxial waveguide modes.

Manuscript received July 13, 1990; revised August 15, 1991. This work is supported by the Department of the Navy under Air Force Contract F19628-85-C-0002.

The author is with the MIT Lincoln Laboratory, 244 Wood Street, Lexington, MA 02173.

IEEE Log Number 9105447.